PHYSICAL REVIEW B **92**, 241305(R) (2015)

Efficient formation of excitons in a dense electron-hole plasma at room temperature

Andreas Hangleiter,[1,*] Zuanming Jin,[2,3] Marina Gerhard,[4] Dimitry Kalincev,[4] Torsten Langer,[1] Heiko Bremers,[1] Uwe Rossow,[1] Martin Koch,[4] Mischa Bonn,[2] and Dmitry Turchinovich[2,†]

[1]*Institut für Angewandte Physik, Technische Unversität Braunschweig, Mendelssohnstrasse 2, 38106 Braunschweig, Germany*

[2]*Max Planck Institute for Polymer Research, Ackermannweg 10, 55128 Mainz, Germany*

[3]*Department of Physics, Shanghai University, 99 Shangda Road, Shanghai 200444, People's Republic of China*

[4]*Fachbereich Physik, Philipps-Universität Marburg, Renthof 5, 35032 Marburg, Germany*

(Received 7 May 2015; published 28 December 2015)

Commonly, excitons in semiconductors are regarded as a low-temperature, low carrier density phenomenon, becoming unstable as the temperature and carrier density increase. Contrary to the common expectation, our ultrafast conductivity and luminescence measurements in GaInN/GaN quantum wells reveal a highly efficient formation of radiative excitons from a high-density electron-hole plasma at room temperature, and provide a quantitative measure of the exciton fraction to reach more than 40% at a total carrier population as high as $\sim 10^{13}$ cm^{-2}. Driven by the mass action of electrons and holes, this effect is believed to contribute to the extraordinarily high quantum efficiency of group-III nitride light emitters.

DOI: 10.1103/PhysRevB.92.241305 PACS number(s): 71.35.Lk, 72.20.Jv, 73.21.−b, 78.47.jh

Room-temperature electronic properties of semiconductors and semiconductor nanostructures, especially at higher charge densities, are commonly discussed in terms of single-particle excitations—free electrons and holes. Many-particle effects, such as the formation of excitons—electron-hole pairs bound by their Coulomb interaction—are usually seen as low-temperature and low-density phenomena.

This is caused by the characteristic energy and length scales, given by the excitonic binding energy $E_b^X = \mu^* e^4/2\varepsilon^2\hbar^2$ and Bohr radius $a_B = \varepsilon\hbar^2/\mu^* e^2$, where $\mu^* = m_e m_h/(m_e + m_h)$ is the exciton reduced mass, m_e and m_h are the effective electron and hole masses, respectively, and ε is the material static dielectric constant. For most semiconductors, such as GaAs, E_b^X is of the order of a few meV [1], thus a room-temperature thermal energy of 26 meV is sufficient to render the Coulomb interaction negligible. In addition to the effect of thermal energy, many-particle effects such as the screening of Coulomb interaction by free electrons and holes [2] as well as Pauli blocking [3] come into play. Consequently, bound electron-hole states can exist only below the Mott density [4] $N \sim a_B^{-i}$, where $i = 3,2,1$ is the system dimensionality for bulk, quantum well (QW), and quantum wire, respectively. For GaAs with $a_B = 11$ nm, this critical density is about $N \sim 10^{18}$ cm^{-3} for bulk material or $N \sim 10^{12}$ cm^{-2} for QWs.

At the same time, excitons provide a highly efficient radiative decay channel for electrons and holes, and efficient exciton formation would lead to an increase in quantum efficiency of optoelectronic devices such as light-emitting diodes (LEDs). Yet, these devices typically operate at injection densities and temperatures so high that efficient exciton formation is believed to be impossible.

In this Rapid Communication we show that under conditions typical for wide-gap semiconductors such as used in blue-green LEDs or lasers, radiative excitons are not only efficiently formed at high carrier densities approaching the Mott density and at room temperature, but that exciton formation is in fact *stimulated* by the increase in electron-hole plasma density. To this end, our results allow one to revisit the traditionally accepted plasma-exciton phase diagram, where the excitons dominate at low carrier density and temperature, and an increase in either parameter leads to exciton dissociation into a free plasma. For GaInN/GaN QWs we quantitatively determine the fraction of excitons in a carrier population, formed in a matter of a few picoseconds, to be more than 40% at carrier densities close to $N \sim 10^{13}$ cm^{-2}.

In our experiments we studied the ultrafast dynamics of the electron-hole plasma and radiative excitons in optically excited $Ga_{0.8}In_{0.2}N$/GaN multiple quantum wells (MQWs) at room temperature. Our samples (wurtzite, grown on *c*-axis sapphire by low-pressure metal-organic vapor phase epitaxy) contained ten GaInN QWs of identical thickness, separated by 7.2 nm GaN barriers. Three samples were studied with QW thicknesses L_z of 2.4, 3.6, and 4.8 nm. The MQWs were excited by 100 fs laser pulses of 400 nm central wavelength, corresponding to a photon energy of 3.1 eV, sufficient for an excitation of the electron-hole transition within the GaInN QWs, but not in the GaN barriers of our samples. We used a variable pumping fluence up to 0.65 mJ/cm^2, leading to a maximum photoexcited carrier density in the QWs of about $N \approx 5 \times 10^{12}$ cm^{-2} per quantum well.

The electron-hole plasma dynamics in photoexcited GaInN/GaN MQWs was probed using time-resolved terahertz (THz) spectroscopy (TRTS). Performed in a traditional normal-incidence transmission configuration, TRTS provides information about the transient evolution of the high-frequency *in-plane* conductivity σ of the photoexcited sample, as free electrons and holes are strong absorbers of THz radiation, while neutral excitons interact only weakly with THz waves [5,6]. For the TRTS photoconductivity measurements single-cycle THz pulses of approximately 300 fs duration were used, with their spectrum covering the frequency range $\sim$0.5–2.5 THz. The THz frequency-resolved photoconductivity spectra at all pump-probe time delays are predominantly real valued, indicative of a conductivity by free charges, and are spectrally flat over most of the THz probe spectral bandwidth [7], indicating a sub-20-fs electron momentum scattering

*a.hangleiter@tu-braunschweig.de
†turchino@mpip-mainz.mpg.de

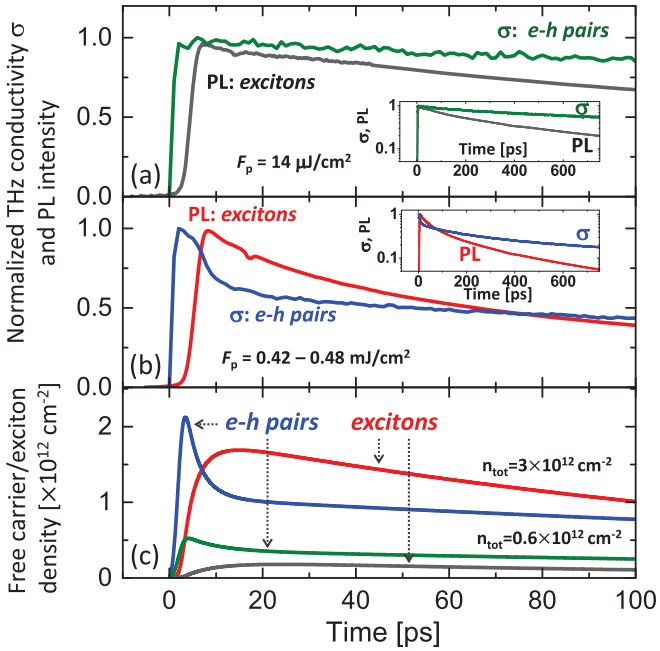

FIG. 1. (Color online) Time-resolved THz photoconductivity and photoluminescence intensity at (a) low and (b) high pump fluence. (c) Simulated free electron-hole and exciton densities after pulsed excitation for two different absorbed photon densities. The insets show the experimental results on a longer time scale.

time. Owing to the mostly real-valued, spectrally flat THz photoconductivity response of the MQWs, the dynamics of the in-plane free-charge conductivity σ can be obtained by simply recording the time dependence of the pump-induced differential transmission at the peak of the THz pulse through the sample [5,8]. The conductivity dynamics observed in this work is predominantly that of electrons rather than holes, owing to a much lighter electron effective mass in GaN, $m_e = 0.2m_0$ as opposed to $m_h = 2.0m_0$ (m_0 is the electron rest mass) [9]. The time resolution in our TRTS experiments was about 0.5 ps.

Time-resolved photoluminescence (TRPL) is a complementary way to study the dynamics of photoexcited electron-hole pairs. Our TRPL measurements were performed using a Hamamatsu M6860 streak camera and a Bruker 25015 monochromator, with the PL signal spectrally integrated over the whole QW emission spectrum. The time resolution in our TRPL experiments was 2 ps, which allowed us to monitor the luminescence dynamics in photoexcited GaInN/GaN MQWs on a time scale similar to the transient conductivity. Our TRTS and TRPL measurements were performed in two different laboratories, while keeping the 400 nm laser excitation fluences very similar for both kinds of measurements.

In Fig. 1 we show typical results of our measurements. In Figs. 1(a) and 1(b) the dynamics of the THz conductivity σ and the PL intensity are shown for a MQW with $L_z = 2.4$ nm, excited at low and high pump fluence, respectively. For the low-fluence excitation $F_p = 14\ \mu\text{J/cm}^2$ shown in Fig. 1(a), the conductivity σ reaches its maximum within ~1 ps after photoexcitation. At the same time, the PL signal reaches its maximum within ~8 ps. We note that this time scale is not limited by the 2-ps temporal resolution of our TRPL measurements. Both the transient conductivity σ and the PL have slow decay dynamics with typical time constants of hundreds of picoseconds. The response changes drastically as the excitation fluence increases. In Fig. 1(b) we show the photoconductivity and PL dynamics measured at higher excitation fluences of 0.48 and 0.42 mJ/cm^2, respectively. The TRPL signal still decays relatively slowly, although somewhat faster than in the case of weaker excitation. At the same time, the conductivity σ develops a pronounced initial fast decay component, not present at weaker excitation in Fig. 1(a). Within this fast decay peak the conductivity is reduced by as much as ~40% from its maximum within only ~10 ps, i.e., the strongly photoexcited system rapidly loses its conductivity while the PL dynamics is not significantly affected. The conductivity and TRPL data taken at intermediate pump fluences vary in between, and are presented in Ref. [7] along with the analysis of the PL spectra. All three samples show a very similar TRPL and conductivity response, which we quantitatively summarize later in the text.

The fast initial conductivity decay cannot be attributed to time-dependent mobility as no large temporal variation in carrier momentum relaxation time is found [7]. Fast recombination processes, such as Auger recombination, may also be ruled out, given the absence of a corresponding fast decay in the PL. Rather, the PL signal rises on a similar time scale as the conductivity decays.

While only charged particles, i.e., free electrons and holes, can contribute to conductivity, both free and bound carriers (i.e., excitons) can contribute to the luminescence (see, e.g., Ref. [10]). Importantly, except for the highest carrier densities, excitons have a *much higher* radiative recombination probability than free electrons and holes [11].

Thus, the very fast initial decay of the free-carrier conductivity at stronger photoexcitation, shown in Fig. 1(b), in conjunction with the delayed rise of the PL, point to a rapid formation of a neutral exciton phase in the photoexcited electron-hole plasma, stimulated by the *increase* in the density of the plasma itself. The results of a simple model, detailed below, accounting for the density-dependent interconversion of free charges and excitons [Fig. 1(c)], capture all key features of the data: At a low injected plasma density $n_{\text{tot}} = 0.6 \times 10^{12}$ cm^2 the dynamics of the density of free carriers and excitons is reminiscent of the dynamics of conductivity and PL, respectively, observed in the case of weak photoexcitation [Fig. 1(a)]. For a higher density $n_{\text{tot}} = 3.0 \times 10^{12}$ cm^2, the plasma and exciton density dynamics now resemble the conductivity and PL measurements taken at a higher excitation fluence [Fig. 1(b)]. In particular, the fast initial decay of the free electron-hole plasma density, caused by rapid exciton formation, and a somewhat faster exciton decay are well reproduced by the calculation.

We summarize the conductivity dynamics in Fig. 2. Figure 2(a) shows the typical conductivity dynamics for the MQW with $L_z = 2.4$ nm, here excited at a pump fluence of $F_p = 0.48$ mJ/cm^2. Provided that the THz conductivity signal is proportional to the free-carrier density, the initial peak signal $\Delta\sigma_p$ is a measure of the total carrier density, and the remaining signal $\Delta\sigma_p - \Delta\sigma_X$ without the fast component gives the quasiequilibrium free-carrier density. The fast decay

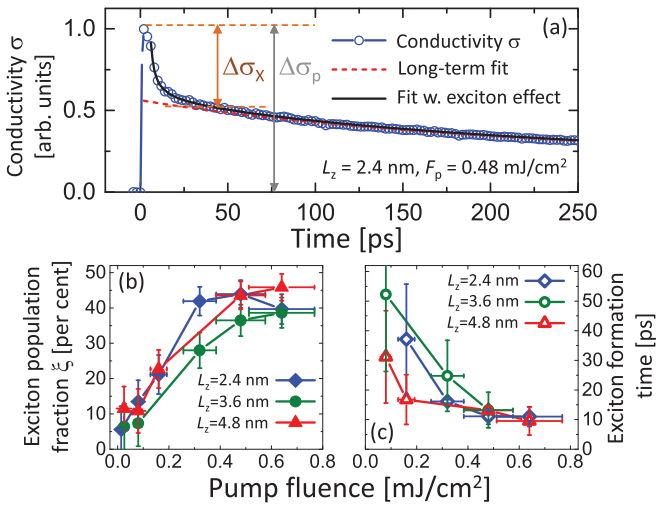

FIG. 2. (Color online) (a) A typical measured conductivity decay dynamics. (b) Exciton population fraction and (c) exciton formation time extracted from the conductivity signals as shown in (a). The dependencies in (b) and (c) are not correlated with the QW width, indicating that exciton formation is a generic material property.

represents the exciton formation and its height is thus a measure of the exciton density. The amplitudes and decay times associated with these processes can be readily extracted from the data assuming a simple phenomenological fit function [7], as exemplified in Fig. 2(a). Figure 2(b) shows the fluence-dependent exciton population fraction defined as the ratio $\xi = \Delta\sigma_X/\Delta\sigma_p$ for the samples with different QW widths, and Fig. 2(c) shows exciton formation dynamics [7]. Within the variation of extracted values, the pump fluence dependency of both exciton population fractions in the photoexcited electron-hole plasma and the exciton formation dynamics reveals no systematic trend with QW width, being similar for all three samples with QW widths $L_z = 2.4$, 3.6, and 4.8 nm. As the excitation fluence increases, the exciton fraction in the photoexcited electron-hole plasma increases from 5% to 10% at the weakest excitation to the saturated value of ∼40% at the strongest pump. At the same time, the exciton formation time decreases from ∼50 ps down to ∼10 ps.

These experimental observations can be consistently explained by considering the following picture of exciton formation from free electrons and holes. The 100 fs laser pulse primarily creates unbound electron-hole pairs with an excess energy (with respect to the QW exciton ground state) of more than 200 meV. These electron-hole pairs are fully contributing to the THz photoconductivity. However, the electron-hole pairs also quickly form (free) neutral excitons, and the exciton formation rate R is nonlinear in the carrier density: It is proportional to the *product* of electron and hole densities $R \propto np$. The formation of excitons proceeds until a quasiequilibrium (given by temperature and carrier densities—see below) is reached. The free-carrier and exciton population in this quasiequilibrium state is still subject to radiative and nonradiative recombination. Only the quasiequilibrium free carriers contribute to the conductivity at longer times.

On the other hand, the luminescence is largely due to excitons. Thus the luminescence exhibits no fast initial decay, but rather a somewhat slower rise, associated with exciton formation, and a subsequent decay due to recombination [12]. The long-term luminescence decay appears faster than the conductivity decay as the quasiequilibrium exciton density is proportional to the product of electron and hole densities. Thus the exciton luminescence intensity is proportional to the product of electron and hole densities (as would be free-carrier luminescence), while the conductivity is a linear function of the free-carrier densities.

In a quantitative picture, the equilibrium between excitons and an electron-hole plasma can be approximated by a law of mass action (Saha equation),

$$\frac{np}{x} = C(T), \tag{1}$$

with n, p and x being the free-carrier and exciton densities, respectively. The equilibrium constant in a two-dimensional system is given by $C(T) = \frac{4\pi\mu^* kT}{h^2} \exp[-\frac{E_b^X}{kT}]$. For μ^* we use a linear interpolation between GaN ($m_e^* = 0.2m_0, m_h^* = 2.0m_0$ [9,13]) and InN ($m_e^* = 0.07m_0, m_h^* = 0.4m_0$ [14]).

Employing the fact that the total density of electron-hole pairs N (free carriers plus excitons) is determined by the excitation laser pulse, the equilibrium exciton fraction ξ can be expressed as $\xi = 1 - \frac{C(T)}{2N}(\sqrt{1 + \frac{4N}{C(T)}} - 1)$.

Finally, the dynamics of exciton formation including recombination can be described by a set of coupled rate equations (assuming equal electron and hole densities for purely optical excitation)

$$\frac{dn}{dt} = G(t) - c_1 n^2 + c_1 C(T)x - \text{recombination terms}, \tag{2}$$

$$\frac{dx}{dt} = c_1 n^2 - c_1 C(T)x - \text{recombination terms}, \tag{3}$$

where c_1 is the formation rate constant for excitons and $G(t)$ is the generation rate.

The result of a simulation based on these rate equations is shown in Fig. 1(c). Indeed, just as in the experiment, at a higher injection level the plasma density exhibits a fast initial decay due to exciton formation, followed by a slower one due to recombination. The exciton density shows a relatively slow rise corresponding to the fast free-carrier decay. Later on, the exciton density also exhibits a slow decay, but following the square of the free-carrier density.

In order to further test the validity of our simple model, we compare the measured and calculated exciton population fraction ξ. In Fig. 3 we plot the value of ξ for the sample with $L_z = 2.4$ nm [same as in Fig. 2(b)] as a function of the photoexcited free-carrier density. The carrier densities have been determined from the experimental pump fluence following Ref. [12] and taking into account the excitonic enhancement of absorption [15,16].

In the same figure, the calculations for the exciton population fraction based on the law of mass action [Eq. (1)] as well as calculations for a correlated many-body system [7] are shown. These calculations consider in-well screening of the polarization field by photogenerated carriers [17–19], include a field-dependent exciton binding energy [20], and take into account carrier redistribution in a polarized MQW structure, giving rise to carrier-density-dependent spatial separation of

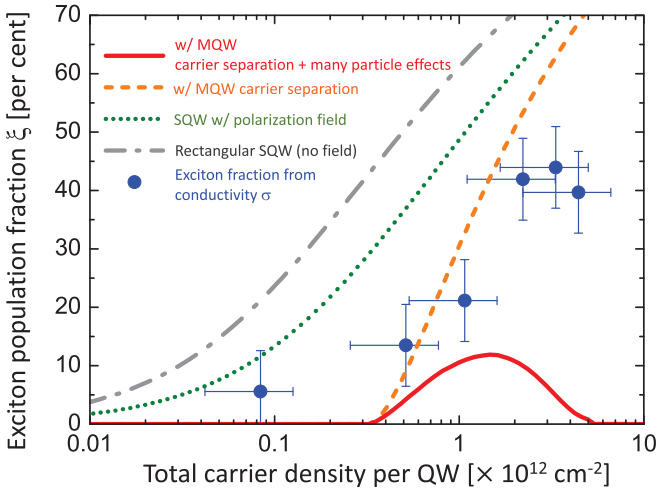

FIG. 3. (Color online) Exciton population fraction extracted from the THz conductivity measurements as a function of carrier density for the 2.4 nm sample (symbols), compared to calculations based on the law of mass action (lines). The solid line represents the full MQW calculation, and the dashed line is without free-carrier screening of the Coulomb interaction. The dotted line is for a single polarized QW and the dashed-dotted line is for a simple rectangular QW.

electrons and holes within the whole MQW structure (Fig. 3, dashed line), as well as including many-particle effects [4,21–23] (Fig. 3, solid line). For comparison, Fig. 3 also shows the result of the calculation based on the law of mass action alone, performed for simple structures—a single polarized QW (dotted line), and a field-free, rectangular QW (dashed-dotted line).

As one can see from Fig. 3, the experimental results show that, even at room temperature, an exciton fraction of almost 50% is obtained in QWs, particularly at rather high carrier densities. The calculation for the cases of single QWs based on the law of mass action Eq. (1) (dotted and dashed-dotted lines in Fig. 3) appears to be a reasonably good approximation as it indeed shows a growing population fraction of excitons as the carrier density increases, while somewhat overestimating the value of ξ. Nevertheless, even such a simplified model captures all the essential physics, namely, the *increase* in exciton fraction with increasing plasma density. When the details of the $Ga_{0.8}In_{0.2}N$/GaN MQW band structure are included, leading to partial carrier separation to the top and bottom QWs [7], the agreement between the data and the model is fairly decent, in particular, reproducing the thresholdlike behavior of the exciton population fraction at densities around 3×10^{11} cm^{-2} (dashed line in Fig. 3).

We note that the exciton fraction obtained using the full many-body calculation [7] (solid line in Fig. 3) significantly underestimates the experimental values, for the following reason. As these calculations are based on a pure two-dimensional (2D) model considering only a single subband, a relatively large phase space volume is occupied at a given carrier density. In reality, several subbands need to be taken into account, reducing the blocked phase space volume and thus reducing the effect of Coulomb screening and Pauli blocking.

Let us consider our results in the framework of previous studies of excitons and free carriers using ultrafast THz spectroscopy. In materials such as GaAs and Si, with exciton binding energies of the order of a few meV, intraexcitonic dipole-allowed transitions (such as, e.g., $1s-2p$ or $1s$-continuum) can be probed resonantly at THz frequencies (1 THz $\equiv$ 4.1 meV). In this fashion, the dynamics of both the plasma and the excitons can be successfully revealed in a single THz experiment [24–27], performed at cryogenic temperatures. Kaindl *et al.* [24,25] and Suzuki and Shimano [26,27] have shown that in conventional semiconductor materials, such as GaAs or Si, excitons only exist at low temperatures and at low carrier densities. High temperature or density leads to exciton dissociation and the formation of a conductive electron-hole plasma.

However, wide-gap semiconductors such as the group-III nitrides used here feature large electron and hole effective masses $m_{e,h}$, and a low static dielectric constant ε, leading to exciton binding energies of some $E_b^X \approx 25$ meV even for bulk material, and a few-nm Bohr radius. Much higher binding energies can be achieved in low-dimensional structures due to additional quantum confinement. As a result, the excitons become more robust at elevated temperatures, and a much higher Mott screening density could be expected. Indeed, for GaN-based QWs used here, with $E_b^X \approx 20$–50 meV [20,28] and $a_B = 2.7$ nm [29], the existence of stable excitons at room temperature, and at carrier densities one order of magnitude higher than in GaAs-based systems, becomes possible. As a result, the exciton formation process is dominated by the *density-enhanced* exciton formation rate $R \propto np$. Under these conditions, the large density of compact excitons strongly increases the radiative recombination probability and adds to the remarkably high quantum efficiency of group-III nitride-based light emitters.

In conclusion, we have demonstrated a regime of rapid formation of an insulating excitonic phase at room temperature in a semiconductor, *stimulated* by an increasing density of electron-hole plasma, i.e., by the mass action of electrons and holes. Our observations are in good agreement with a simple parameter-free model describing the coexistence of conductive and insulating phases in a semiconductor.

The authors acknowledge Professor J. M. Hvam and Professor B. S. Monozon for fruitful discussions and comments on the manuscript, Dr. H. Porte, Professor J. I. Dijkhuis, and Professor P. U. Jepsen for their contributions at the early stages of this work, and the European Union Marie Curie Program (Career Integration Grant No. 334324 "LIGHTER") and Max Planck Society for financial support.

[1] D. D. Sell, Phys. Rev. B **6**, 3750 (1972).
[2] C. Klingshirn and H. Haug, Phys. Rep. **70**, 315 (1981).
[3] M. Schmidt and G. Röpke, Phys. Status Solidi B **139**, 441 (1987).
[4] N. F. Mott, Rev. Mod. Phys. **40**, 677 (1968).
[5] R. Ulbricht, E. Hendry, J. Shan, T. F. Heinz, and M. Bonn, Rev. Mod. Phys. **83**, 543 (2011).

[6] F. Wang, J. Shan, M. A. Islam, I. P. Herman, M. Bonn, and T. F. Heinz, Nat. Mater. **5**, 861 (2006).
[7] See Supplemental Material at http://link.aps.org/supplemental/10.1103/PhysRevB.92.241305 for a description of (i) the details of THz frequency-resolved conductivity, (ii) conductivity and PL decay data at intermediate pump fluences as well as their analysis, and (iii) details of many-particle calculations of the degree of ionization of excitons.
[8] K. P. H. Lui and F. A. Hegmann, Appl. Phys. Lett. **78**, 3478 (2001).
[9] J. S. Im, A. Moritz, F. Steuber, V. Härle, F. Scholz, and A. Hangleiter, Appl. Phys. Lett. **70**, 631 (1997).
[10] J. M. Hvam, Phys. Rev. B **4**, 4459 (1971).
[11] B. K. Ridley, Phys. Rev. B **41**, 12190 (1990).
[12] T. Langer, A. Chernikov, D. Kalincev, M. Gerhard, H. Bremers, U. Rossow, M. Koch, and A. Hangleiter, Appl. Phys. Lett. **103**, 202106 (2013).
[13] B. K. Meyer, D. Volm, A. Graber, H. C. Alt, T. Detchprohm, K. Amano, and I. Akasaki, Solid State Commun. **95**, 597 (1995).
[14] W. Walukiewicz, J. W. Ager, K. M. Yu, Z. Liliental-Weber, J. Wu, S. X. Li, R. E. Jones, and J. D. Denlinger, J. Phys. D: Appl. Phys. **39**, R83 (2006).
[15] R. Elliott, Phys. Rev. **108**, 1384 (1957).
[16] M. Shinada and S. Sugano, J. Phys. Soc. Jpn. **21**, 1936 (1966).
[17] J. C. Harris, S. Kako, T. Someya, and Y. Arakawa, Phys. Status Solidi B **216**, 423 (1999).
[18] F. della Sala, F. Bernardini, V. Fiorentini, R. Scholz, J. M. Jancu, A. di Carlo, and P. Lugli, Appl. Phys. Lett. **74**, 2002 (1999).
[19] P. J. S. van Capel, D. Turchinovich, H. P. Porte, S. Lahmann, U. Rossow, A. Hangleiter, and J. I. Dijkhuis, Phys. Rev. B **84**, 085317 (2011).
[20] P. Bigenwald, P. Lefebvre, T. Bretagnon, and B. Gil, Phys. Status Solidi B **216**, 371 (1999).
[21] J. Lee, H. N. Spector, and P. Melman, J. Appl. Phys. **58**, 1893 (1985).
[22] F. Stern and W. Howard, Phys. Rev. **163**, 816 (1967).
[23] A. Hangleiter, Phys. Rev. B **48**, 9146 (1993).
[24] R. A. Kaindl, M. A. Carnahan, D. Hägele, R. Lövenich, and D. S. Chemla, Nature (London) **423**, 734 (2003).
[25] R. A. Kaindl, D. Hägele, M. A. Carnahan, and D. S. Chemla, Phys. Rev. B **79**, 045320 (2009).
[26] T. Suzuki and R. Shimano, Phys. Rev. Lett. **103**, 057401 (2009).
[27] T. Suzuki and R. Shimano, Phys. Rev. Lett. **109**, 046402 (2012).
[28] S. Lahmann, F. Hitzel, U. Rossow, and A. Hangleiter, Phys. Status Solidi C **0**, 2202 (2003).
[29] G. Steude, B. K. Meyer, A. Göldner, A. Hoffmann, F. Bertram, J. Christen, H. Amano, and I. Akasaki, Appl. Phys. Lett. **74**, 2456 (1999).